The Journal of Chemical Physics

RESEARCH ARTICLE | JANUARY 30 2024

# Liouvillian exceptional points of an open driven two-level system FREE

Nikhil Seshadri ; Anqi Li ; Michael Galperin



*J. Chem. Phys.* 160, 044116 (2024)
https://doi.org/10.1063/5.0177714







The Journal of Chemical Physics ARTICLE pubs.aip.org/aip/jcp

# Liouvillian exceptional points of an open driven two-level system

Cite as: J. Chem. Phys. 160, 044116 (2024); doi: 10.1063/5.0177714
Submitted: 23 September 2023 • Accepted: 5 January 2024 •
Published Online: 30 January 2024



Nikhil Seshadri,[1] Anqi Li,[2] and Michael Galperin[2,a)]

## AFFILIATIONS

[1] Harvard University, Cambridge, Massachusetts 02138, USA
[2] Department of Chemistry and Biochemistry, University of California San Diego, La Jolla, California 92093, USA

[a)] **Author to whom correspondence should be addressed:** migalperin@ucsd.edu

## ABSTRACT

We study the applicability of the Liouvillian exceptional points (LEPs) approach to nanoscale open quantum systems. A generic model of the driven two-level system in a thermal environment is analyzed within the nonequilibrium Green's function (NEGF) and Bloch quantum master equation formulations. We derive the latter starting from the exact NEGF Dyson equations and highlight the qualitative limitations of the LEP treatment by examining the approximations employed in its derivation. We find that the non-Markov character of evolution in open quantum systems does not allow for the introduction of the concept of exceptional points for a description of their dynamics. Theoretical analysis is illustrated with numerical simulations.





## I. INTRODUCTION

Non-Hermitian quantum mechanics[1] is an accepted way of treating open quantum systems and is employed in many fields of theoretical research, from optics, opto-mechanics, and polaritonics to quantum field theory, molecular physics, and quantum transport. The complex values of operator spectra in these considerations reflect the non-stationary character of system states, with the balance between gain and loss accounted for by the imaginary parts of eigenvalues. The most non-trivial physics (such as unidirectional transport, anomalous lasing and absorption, and chiral modes) takes place at and in the vicinity of the degeneracies of the complex eigenvalues—exceptional points (EPs).

Experimentally, EP behavior has been observed mostly in optics,[2] in the setting of a chaotic optical microcavity,[3] optical coupled systems with a complex index potential,[4] and photonic lattices.[5] EP systems were suggested as a platform for the development of topological optoelectronics.[6,7] Recently, observations of EPs in single-spin systems (nitrogen-vacancy centers in diamonds) were also reported.[8] The sensitivity of EP system responses to parameter changes led to suggestions of employing EP systems as optical[9,10] and quantum[11] sensors. The decoherence enhancement observed in the vicinity of EPs[12,13] opens a way for the exploration of EPs for quantum information processing. EP physics was also observed in polaritonic systems (exciton–polaritons in semiconductor microcavities)[14] and in thermal transport (chiral heat transport).[15]

The majority of theoretical considerations use effective non-Hermitian Hamiltonians as operators describing EP physics.[16–28] These operators are formed by adding complex absorbing potentials (retarded and/or advanced projections of self-energies) to the Hermitian system Hamiltonians. Their degeneracies, the Hamiltonian EPs (HEPs), are the focus of these studies.

Another non-Hermitian operator describing the evolution of open quantum systems is the Liouvillian. Its degeneracies, Liouvillian EPs (LEPs), were also discussed recently.[29–33] Analytical studies comparing HEPs and LEPs conclude that the two types of EPs have essentially different properties and that they become equivalent only in the semiclassical limit. Similar to HEPs, Liouvillian-based analysis predicts non-trivial behavior at or in the vicinity of LEPs. For example, LEPs were shown to represent a threshold between diffusive and ballistic motion in a 1d quantum Lorentz gas.[34,35] Enhancement of decoherence rate,[36–38] the possibility of chiral state transfer,[39] and optimization of steering toward a predesigned target state[40] are predicted in the presence of LEPs. Finally, a recent experiment demonstrated enhanced performance of the single-ion quantum heat engine from the LEPs.[41]

Recently, we studied the applicability of the concept of HEPs in nanoscale open quantum systems.[42] Utilizing a model of two vibrational modes in a cavity, we compared standard nonequilibrium Green's function (NEGF) with HEP-based predictions. We derived the latter from the former and discussed the approximations required to reduce the exact NEGF to an approximate HEP description. In particular, we showed that HEP disregards lesser and greater projections of self-energy due to intra-system interactions while keeping its retarded projection, which makes the HEP treatment inconsistent and may lead to qualitative failures. Another limiting factor of the HEP approach is its Markov character.

Here, we present an analysis of LEP-based considerations, starting with the exact NEGF treatment and exploring the approximations necessary to reduce the latter to the approximate LEP description. The two most basic and widely employed models for LEP analysis are the driven two-level system (TLS)[43–45] and the oscillator[46] in a generic environment. We use the TLS as a model for comparison between the NEGF and LEP methods. Similar to our findings in Ref. 42, LEP is also limited by its Markov character. Nevertheless, contrary to the HEP, the Liouvillian-based treatment disregards the retarded projection of the self-energies while keeping their lesser and greater projections. Some limitations in the applicability of LEP methods to nanoscale open quantum systems are illustrated with simulations comparing the NEGF and Bloch quantum master equation (QME) results for driven TLS in a thermal environment.

In Sec. II, we introduce the model and present its NEGF treatment. We then utilize NEGF as a starting point for the derivation of the Bloch QME and its generalization, which accounts for dissipation, and discuss the approximations necessary to reduce the exact NEGF treatment to an approximate Redfield/Lindblad QME. Section III compares the results of numerical simulations performed within the NEGF formulation and within the two types of Bloch QME formulations. Conclusions are drawn in Sec. IV.

## II. DRIVEN TLS IN A THERMAL ENVIRONMENT

### A. Model

We consider a two-level system that is driven by the external classical field $E(t)$ and dissipated by a thermal bath. The latter is a continuum of Bose modes $\{\alpha\}$ (Fig. 1). The Hamiltonian of this model is

$$\hat{H}(t) = \hat{H}^S(t) + \hat{H}^B + \hat{V}^{SB}, \tag{1}$$

where $\hat{H}^S(t)$ and $\hat{H}^B$ describe the decoupled system and bath, respectively. $\hat{V}^{SB}$ is the system-bath coupling. Explicit expressions for each of the terms are given by

$$\begin{aligned} \hat{H}^S(t) &= \sum_{i=1,2} \varepsilon_i \hat{d}_i^\dagger \hat{d}_i - \mu E(t)\left(\hat{d}_1^\dagger \hat{d}_2 + \hat{d}_2^\dagger \hat{d}_1\right), \\ \hat{H}^B &= \sum_\alpha \omega_\alpha \hat{b}_\alpha^\dagger \hat{b}_\alpha, \\ \hat{V}^{SB} &= \sum_{i,j=1,2} \sum_\alpha \left( V_{ij,\alpha}\left[\hat{d}_i^\dagger \hat{d}_j\right]^\dagger \hat{b}_\alpha + V_{\alpha,ij}\, \hat{b}_\alpha^\dagger \left[\hat{d}_i^\dagger \hat{d}_j\right]\right). \end{aligned} \tag{2}$$

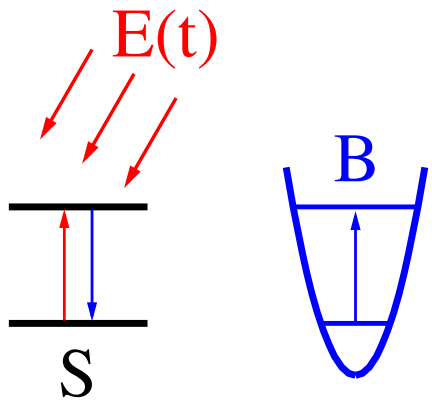


**FIG. 1.** Sketch of a model for optically driven two-level system (S) in thermal environment (B).

Here, $\hat{d}_i^\dagger$ ($\hat{d}_i$) and $\hat{b}_\alpha^\dagger$ ($\hat{b}_\alpha$) create (annihilate) an electron in level $i$ and an excitation in mode $\alpha$, respectively. $\mu$ is the transition dipole moment. The driving field is taken to be harmonic

$$E(t) = E_0 \cos(\omega_0 t). \tag{3}$$

In the following analysis, we assume $\varepsilon_1 < \varepsilon_2$ and consider coupling to the thermal bath in the rotating-wave approximation (RWA); that is, $V_{21,\alpha} = V_{\alpha,21} = 0$. We note that the RWA is central to the derivation of the Bloch QME.

### B. NEGF formulation

Within the NEGF formulation, the central quantity of interest is the single-particle Green's function of the system defined on the Keldysh contour

$$G_{ij}(\tau_1, \tau_2) \equiv -i\langle T_c\, \hat{d}_i(\tau_1)\, \hat{d}_j^\dagger(\tau_2)\rangle. \tag{4}$$

Here, $T_c$ is the contour ordering operator, $\tau_{1,2}$ are the contour variables, and the creation (annihilation) operator $\hat{d}_j^\dagger(\tau_2)$ [$\hat{d}_i(\tau_1)$] is in the Heisenberg picture. Knowledge of $G_{ij}(\tau_1, \tau_2)$ allows for the calculation of the characteristics of the system and its responses to external perturbations. In particular, in the single-electron subspace of the problem, the system density matrix is given by the lesser projection of Green's function (4) taken at equal times,

$$\rho_{ij}(t) = -i\, G_{ij}^<(t, t). \tag{5}$$

This relation is central to the comparison between the NEGF and Bloch quantum master equation (QME) results.

The dynamics of the system is described by the Dyson equation for Green's function (4)

$$\begin{aligned} i\frac{\partial}{\partial \tau_1} G_{ij}(\tau_1, \tau_2) &= \delta_{i,j}\, \delta(\tau_1, \tau_2) + \sum_{n=1,2} H_{in}^S(t_1)\, G_{nj}(\tau_1, \tau_2) \\ &\quad + \int_c d\tau\, \Sigma_{in}(\tau_1, \tau)\, G_{nj}(\tau, \tau_2), \end{aligned} \tag{6}$$

where $t_1$ is the physical time corresponding to contour variable $\tau_1$ and $\Sigma(\tau_1, \tau)$ is the self-energy due to the coupling of the system to

the bath. While the exact expression for the latter is not accessible due to the many-body character of the system-bath coupling $\hat{V}^{SB}$, an appropriate level of theory for future comparison with the Bloch QME can be achieved by a second-order diagrammatic expansion. Within this (Hartree–Fock) approximation, the expression for the self-energy is (see Appendix A for derivation)

$$\Sigma_{ij}(\tau_1,\tau_2) = \delta(\tau_1,\tau_2)\sum_{n_1,n_2}\int_c d\tau\,\rho_{n_1n_2}(t)[\Pi_{ji,n_2n_1}(\tau_1,\tau) + \Pi_{n_1n_2,ij}(\tau,\tau_1)] + i\sum_{n_1,n_2}[\Pi_{n_1i,n_2j}(\tau_1,\tau_2) + \Pi_{jn_2,in_1}(\tau_2,\tau_1)]G_{n_1n_2}(\tau_1,\tau_2). \tag{7}$$

Here,

$$\Pi_{n_1n_2,n_3n_4}(\tau_1,\tau_2) \equiv \sum_\alpha V_{n_1n_2,\alpha}\,F^{(0)}_\alpha(\tau_1,\tau_2)\,V_{\alpha,n_3n_4}, \tag{8}$$

is the thermal bath-induced effective interaction between transitions $n_1n_2$ and $n_3n_4$ and,

$$F^{(0)}_\alpha(\tau_1,\tau_2) \equiv -i\left\langle T_c\,\hat{b}_\alpha(\tau_1)\,\hat{b}^\dagger_\alpha(\tau_2)\right\rangle_0, \tag{9}$$

is Green's function of free phonon mode $\alpha$ in the bath.

### C. Bloch QME

The derivation of an approximate Redfield/Lindblad QME starts from the exact equation-of-motion (EOM) for the density matrix given by (5), which is derived within the NEGF formulation. The EOM is (see Appendix B for derivation)

$$\frac{d}{dt}\rho_{ij}(t) = i\,\omega_{ji}\,\rho_{ij}(t) - i\,\mu\,E(t)\big[\rho_{\bar{i}j}(t) - \rho_{i\bar{j}}(t)\big] + \sum_{n,n_1,n_2}\int_{-\infty}^{t} dt'\Big[\Pi^{>}_{ni,n_1n_2}(t-t')\,G^{(2)\,<}_{n_1n_2,nj}(t',t) - \Pi^{<}_{ni,n_1n_2}(t-t')\,G^{(2)\,>}_{n_1n_2,nj}(t',t) - \Pi^{>}_{jn,n_1n_2}(t-t')\,G^{(2)\,<}_{n_1n_2,in}(t',t) + \Pi^{<}_{jn,n_1n_2}(t-t')\,G^{(2)\,>}_{n_1n_2,in}(t',t) + G^{(2)\,<}_{ni,n_1n_2}(t,t')\,\Pi^{>}_{n_1n_2,nj}(t'-t) - G^{(2)\,>}_{ni,n_1n_2}(t,t')\,\Pi^{<}_{n_1n_2,nj}(t'-t) - G^{(2)\,<}_{jn,n_1n_2}(t,t')\,\Pi^{>}_{n_1n_2,in}(t'-t) + G^{(2)\,>}_{jn,n_1n_2}(t,t')\,\Pi^{<}_{n_1n_2,in}(t'-t)\Big], \tag{10}$$

where $\bar{i},\bar{j} = 2(1)$ for $i,j = 1(2)$, $\omega_{ji} \equiv \varepsilon_j - \varepsilon_i$ and,

$$G^{(2)}_{n_1n_2,n_3n_4}(\tau_1,\tau_2) \equiv -i\langle T_c\left[\hat{d}^\dagger_{n_1}\hat{d}_{n_2}\right](\tau_1)\left[\hat{d}^\dagger_{n_3}\hat{d}_{n_4}\right]^\dagger(\tau_2)\rangle, \tag{11}$$

is the two-particle Green's function. Reducing the exact EOM (10) to the Redfield/Lindblad QME requires approximating its right side with a Markov dynamics. The Redfield/Lindblad QME can be obtained from the Green's function Dyson equation by employing a Kadanoff–Baym-like ansatz,[47]

$$G^{(2)\gtrless}_{n_1n_2,n_3n_4}(t_1,t_2) \approx \theta(t_1-t_2)\,e^{-i\omega_{21}(t_1-t_2)}\,G^{(2)\gtrless}_{n_1n_2,n_3n_4}(t_2,t_2) + \theta(t_2-t_1)\,e^{-i\omega_{43}(t_1-t_2)}\,G^{(2)\gtrless}_{n_1n_2,n_3n_4}(t_1,t_1), \tag{12}$$

where $\theta(\cdots)$ is the Heaviside step function. Employing this ansatz leads to the Bloch equations (see Appendix C for derivation)

$$\frac{d}{dt}\begin{pmatrix}\rho_{11}(t)\\ \rho_{22}(t)\\ \rho_{12}(t)\\ \rho_{21}(t)\end{pmatrix} = -i\begin{bmatrix} -iW_{2\leftarrow1} & iW_{1\leftarrow2} & \mu E(t) & -\mu E(t)\\ iW_{2\leftarrow1} & -iW_{1\leftarrow2} & -\mu E(t) & \mu E(t)\\ \mu E(t) & -\mu E(t) & -\omega_{21}-iW_d & 0\\ -\mu E(t) & \mu E(t) & 0 & \omega_{21}-iW_d\end{bmatrix}\times\begin{pmatrix}\rho_{11}(t)\\ \rho_{22}(t)\\ \rho_{12}(t)\\ \rho_{21}(t)\end{pmatrix}. \tag{13}$$

Here,

$$W_{2\leftarrow1} \equiv \Gamma_{12,12}(\omega_{21})\,N(\omega_{21}),\qquad W_{1\leftarrow2} \equiv \Gamma_{12,12}(\omega_{21})\,[1+N(\omega_{21})], \tag{14}$$

are the population transfer rates and,

$$W_d \equiv \frac{W_{2\leftarrow1}+W_{1\leftarrow2}}{2} + \frac{\Gamma_{11,11}(0)+\Gamma_{22,22}(0)}{2}[1+2\,N(0)], \tag{15}$$

is the dephasing rate. In Eqs. (14) and (15),

$$\Gamma_{n_1n_2,n_3n_4}(\omega) \equiv 2\pi\sum_\alpha V_{n_1n_2,\alpha}\,V_{\alpha,n_3n_4}\,\delta(\omega-\omega_\alpha), \tag{16}$$

is the dissipation matrix.

Finally, by using (3) with $\omega_0 - \omega_{21} \equiv \Delta \ll \omega_0$, going into the rotating frame of the field

$$\tilde{\rho}_{12}(t) \equiv e^{-i\omega_0 t}\,\rho_{12}(t), \tag{17}$$

and introducing the spin operators

$$\tilde{S}_x(t) \equiv \tilde{\rho}_{21}(t) + \tilde{\rho}_{12}(t),\qquad \tilde{S}_y(t) \equiv i[\tilde{\rho}_{21}(t) - \tilde{\rho}_{12}(t)],\qquad S_z(t) \equiv \rho_{22}(t) - \rho_{11}(t), \tag{18}$$

one can employ the rotating wave approximation (RWA) to express the Bloch QME (13) as an EOM for the spin operator

$$\frac{d}{dt}\begin{pmatrix}\tilde{S}_x(t)\\ \tilde{S}_y(t)\\ S_z(t)\end{pmatrix}=\begin{bmatrix}-\frac{1}{T_2} & \Delta & 0\\ -\Delta & -\frac{1}{T_2} & \mu E_0\\ 0 & -\mu E_0 & -\frac{1}{T_1}\end{bmatrix}\begin{pmatrix}\tilde{S}_x(t)\\ \tilde{S}_y(t)\\ S_z(t)\end{pmatrix}+\begin{pmatrix}0\\ 0\\ \frac{S_z^0}{T_1}\end{pmatrix}. \tag{19}$$

Here,

$$\frac{1}{T_1}\equiv W_{2\leftarrow 1}+W_{1\leftarrow 2},\qquad \frac{1}{T_2}\equiv W_d,$$
$$S_z^0\equiv\frac{W_{2\leftarrow 1}-W_{1\leftarrow 2}}{W_{2\leftarrow 1}+W_{1\leftarrow 2}}. \tag{20}$$

### D. Generalized Bloch QMEs

While deriving the Bloch QME (13) from the exact EOM (10), one loses proper non-Markov evolution and disregards dissipation. Note that while the former is common for Hamiltonian and Liouvillian EP formulations,[42] the latter is specific to Liouvillian EPs. Indeed, the Hamiltonian EP formulation disregards the lesser/greater projections of self-energy, while the ansatz (12) misses the retarded projection; however, the generalized Kadanoff–Baym ansatz (GKBA) in the NEGF literature[47,48] does preserve information about dissipation. To construct the Liouville space analog, we follow the procedure originally introduced in Ref. 49. This leads to (see Appendix D for derivation)

$$G^{(2)\gtrless}_{n_1n_2,n_3n_4}(t_1,t_2)\approx i\sum_{e,f}\Big[\mathcal{G}^r_{n_1n_2,ef}(t_1-t_2)\,G^{(2)\gtrless}_{ef,n_3n_4}(t_2,t_2)-G^{(2)\gtrless}_{n_1n_2,ef}(t_1,t_1)\,\mathcal{G}^a_{ef,n_3n_4}(t_1-t_2)\Big], \tag{21}$$

where

$$\mathcal{G}^r_{n_1n_2,n_3n_4}(t_1,t_2)\equiv -i\theta(t_1-t_2)\langle\langle n_2n_1|\,\mathcal{U}_{\mathit{eff}}(t_1,t_2)\,|n_4n_3\rangle\rangle,$$
$$\mathcal{G}^a_{n_1n_2,n_3n_4}(t_1,t_2)\equiv +i\theta(t_2-t_1)\langle\langle n_2n_1|\,\mathcal{U}^\dagger_{\mathit{eff}}(t_2,t_1)\,|n_4n_3\rangle\rangle, \tag{22}$$

are the retarded and advanced Green's functions in Liouville space, respectively, and

$$\mathcal{U}_{\mathit{eff}}(t_1,t_2)\equiv T\,\exp\Big[-i\int_{t_2}^{t_1}dt\;\mathcal{L}_{\mathit{eff}}(t)\Big], \tag{23}$$

is the Liouville space effective evolution operator, where $\mathcal{L}_{\mathit{eff}}(t)$ defines time evolution in the system subspace of the problem. We note that Eq. (21) is an approximation. The approximation is introduced by employing the projection operator (D3) in exact expressions (D1), which makes (21) a second-order contribution in the infinite diagrammatic expansion of the coupled system-bath evolution in strength of the system-bath coupling.

We employ parts of the Redfield/Lindblad Liouvillian matrix on the right side of Eq. (13) as the system evolution generator. In particular, retaining only free evolution [i.e., disregarding driving $\mu E(t)$ and dissipation $W_{2\leftarrow1}$, $W_{1\leftarrow2}$, and $W_d$] reduces (21) to (12).

Keeping the dissipation, using (21) in (10), and assuming the Born–Markov approximation leads to a generalized version of the Bloch QME, which retains the same form (13), although with renormalized ($\bar{W}$) dissipation rates

$$\bar{W}_{2\leftarrow1}\equiv -i\int\frac{d\omega}{2\pi}\,\Pi^<_{12,12}(\omega)\;\mathrm{Im}\Big[\frac{1}{\omega-\omega_{21}+iW_d}\Big],$$
$$\bar{W}_{1\leftarrow2}\equiv -i\int\frac{d\omega}{2\pi}\,\Pi^>_{12,12}(\omega)\;\mathrm{Im}\Big[\frac{1}{\omega-\omega_{21}+iW_d}\Big],$$
$$\bar{W}_d\equiv -\int\frac{d\omega}{2\pi}\Bigg[\frac{\Pi^<_{11,11}(\omega)+\Pi^>_{22,22}(\omega)}{\omega+iW_d}-\frac{\Pi^>_{11,11}(\omega)+\Pi^<_{22,22}(\omega)}{\omega-iW_d}+\frac{V^R_{11,1}\big[V^R\big]^{-1}_{1,1}\Pi^>_{12,12}(\omega)+V^R_{22,1}\big[V^R\big]^{-1}_{1,2}\Pi^<_{12,12}(\omega)}{\omega-\omega_{21}+i\delta}+\frac{V^R_{11,2}\big[V^R\big]^{-1}_{2,1}\Pi^>_{12,12}(\omega)+V^R_{22,2}\big[V^R\big]^{-1}_{2,2}\Pi^<_{12,12}(\omega)}{\omega-\omega_{21}+i(W_{2\leftarrow1}+W_{1\leftarrow2})}\Bigg]. \tag{24}$$

Here, $\mathbf{V}^R$ is the right eigenvector of the Liouvillian matrix. Note that while keeping driving terms in the effective evolution is possible, we will not pursue this direction because the accepted approach regarding the derivation of the standard Bloch QME requires one to disregard the driving term when deriving dissipators of the Liouvillian. Note also that using the Liouville space generalized Kadanoff–Baym ansatz on the Keldysh anti-contour[50] would lead to the same form of the generalized Bloch equation.

Finally, one can choose to solve the time-nonlocal (non-Markov) version of the QME. Using (21) in (10) without the Born–Markov assumption leads to

$$\frac{d}{dt}\rho_{11}(t)=\mu E(t)\,2\;\mathrm{Im}[\rho_{12}(t)]+2\;\mathrm{Im}\int_{-\infty}^{t}dt'\Big(\Pi^<_{12,12}(t-t')\,\rho_{11}(t')-\Pi^>_{12,12}(t-t')\big[1-\rho_{11}(t')\big]e^{(i\omega_{21}-W_d)(t-t')}\Big),$$
$$\frac{d}{dt}\rho_{12}(t)=i\omega_{12}\rho_{12}(t)-i\mu E(t)[2\rho_{11}(t)-1]-i\int_{-\infty}^{t}dt'\Bigg(\big[\Pi^>_{11,11}(t-t')+\Pi^<_{22,22}(t-t')+\Pi^<_{11,11}(t'-t)+\Pi^>_{22,22}(t'-t)\big]\times e^{(i\omega_{21}-W_d)(t-t')}+\sum_{i=1,2}\Big[V^R_{11,i}\,e^{-i\lambda_i(t-t')}\big[V^R\big]^{-1}_{i,11}\Pi^>_{12,12}(t'-t)+V^R_{22,i}\,e^{-i\lambda_i(t-t')}\big[V^R\big]^{-1}_{i,22}\Pi^<_{12,12}(t'-t)\Big]\Bigg)\rho_{12}(t'). \tag{25}$$

Here, $\lambda_i$ are the eigenvalues of the Liouvillian matrix. We note that the non-Markov version of the Bloch QME, Eq. (25), accounts for the broadening of system states induced by their hybridization with the bath, which is completely missed by the standard Bloch QME, Eq. (13). At the same time, this result is still an approximation (it is only second-order in infinite hybridization expansion).

That is, while for moderate coupling strengths, Eq. (25) can produce relatively accurate results, for significant system-bath coupling strengths, the approximation may fail.

Below, we use Bloch Eq. (13) and its generalizations (24) and (25) to discuss the concept of exceptional points for a Liouville operator. Following Ref. 43, we evaluate the time dependence of the $z$-projection of the spin operator $S_z(t)$ and use it in eigenmode analysis,

$$S_z(t) = \sum_k d_k\, e^{-i\omega_k t}. \tag{26}$$

Degeneracies of the complex eigenmodes $\omega_k$ represent LEPs. As discussed in Ref. 51, the latter can be approximately found from the points of divergence of the absolute values of the coefficients $|d_k|$, although extended analysis is needed for further characterization. We will use the parameters found for LEPs in Ref. 43 as a starting point for our consideration.

## III. NUMERICAL RESULTS

We now evaluate $S_z(t)$ within different methodologies and use the results of simulations to obtain exceptional points for the Liouville operator.

Unless stated otherwise, the parameters of the simulations are the following. The energy levels of the system are $\varepsilon_1 = 0$ and $\varepsilon_2 = 1$, the laser detuning $\Delta \equiv \omega_0 - \omega_{21} = 0.001\,02$, and the coupling to the driving field $\mu\, E_0 = 0.001$. For simplicity, we take $V_{\alpha,11} = V_{\alpha,22} = 0$, so that the dephasing rates are $1/T_1 = 2/T_2 = 0.1$. The temperature of the bath is assumed to be zero. Simulations were performed on a time grid of 200 points with step 1. We confirmed that simulations on a grid of 2000 points with step 0.1 yield similar results.

For non-Markov simulations, we employ the bath spectral function

$$J(\omega) \equiv \left(\frac{\omega}{\omega_{21}}\right)^2 \exp\left[2\left(1 - \frac{\omega}{\omega_{21}}\right)\right], \tag{27}$$

and the bath dephasing rate is defined as

$$\Gamma_{12,12}(\omega) \equiv \Gamma_{12,12}(\omega_{21})\, J(\omega) = J(\omega)/T_1. \tag{28}$$

The Fast Fourier transform is performed on a grid of 10 001 points and utilizes the FFTW library.[52] The NEGF simulations are performed by employing the procedure first introduced in Ref. 53.

Figure 2 shows the time dependence of the $z$-projection of the spin operator after employing the various approaches. Note that the differences in shapes of the curves $S_z(t)$ reflect differences in underlying eigenmode compositions. Note that the differences in the long time value of the projection are due to the renormalization of the dissipation parameters (24) and, therefore, are of secondary importance. Comparing QME and NEGF results [panels (a) and (b), respectively], we note the oscillating behavior of the NEGF stationary state and the difference in magnitude of the signal. The reasons for the discrepancy are assumptions made when deriving the Bloch QME and its generalizations: 1. the rotating wave approximation in external driving; and 2. the neglecting effect of the driving term on the dissipator super-operator (i.e., the dissipator is derived as if there is no driving). Within the NEGF, the driving term is taken into account exactly.

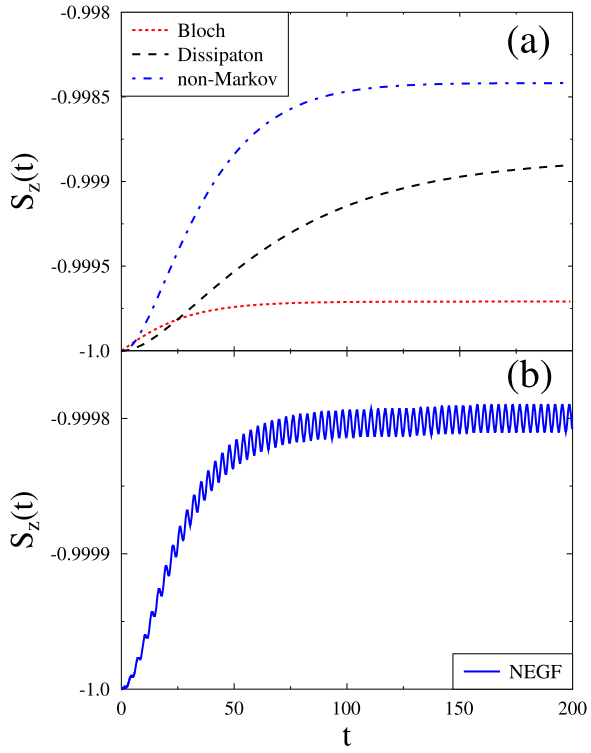


**FIG. 2.** Time dependence of the $z$-component of the spin operator, $S_z(t)$. Panel (a) presents the results of simulations employing the standard Bloch QME, Eq. (19) (dotted line, red); Bloch QME with dissipation included, Eq. (24) (dashed line, black); and non-Markov Bloch QME with dissipation included, Eq. (25) (dashed–dotted line, blue). Panel (b) shows the results of the NEGF Hartree–Fock simulations, Eqs. (5)–(7).

We now turn to the exceptional points analysis of the resulting time series. Because we use the parameters in Ref. 43, we know that our standard Bloch QME simulations are performed in the vicinity of LEPs of second order. Therefore, the divergence of the coefficient $|d_k|$ indicates the presence of an exceptional point. Instead of the harmonic inversion analysis employed in Ref. 43 for eigenmode decomposition, we use its filter diagonalization variant.[54] For the parameters of the simulations, the latter method appears to be more stable.

Figure 3 presents the eigenmode analysis for the time series $S_z(t)$ obtained within different Bloch QME schemes. The divergence of the expansion coefficient $|d_1|$ and the disappearance of the eigenmode difference in the analysis of the standard Bloch QME results presented in panel (a) indicate the presence of a second order LEP at $\mu E_0 \sim 0.025$. Panel (b) shows a similar analysis for generalized Bloch QME with included dissipation. Similar to the standard Bloch QME, three eigenmodes are present in the region away from the LEP. QME rate renormalization, Eq. (24), leads to a shift in the position of the LEP, which now occurs at $\mu E_0 \sim 0.015$. The result of the analysis for the non-Markov QME is shown in panel (c). We find four different eigenmodes in this case. A careful comparison with Markov's consideration of panel (b) shows the absence of exceptional points; one can see that the difference in eigenmodes does not disappear.

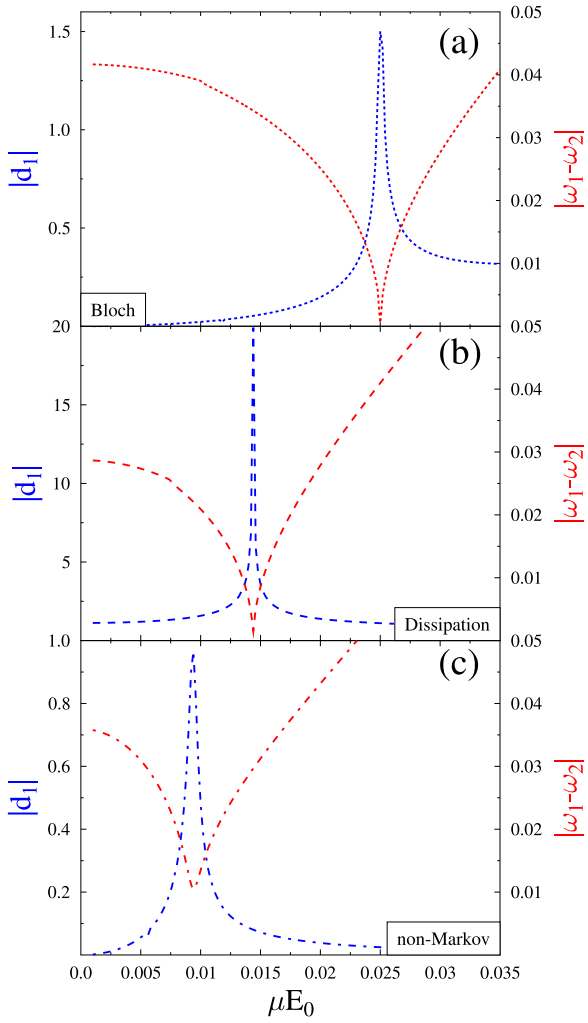


**FIG. 3.** Eigenmode analysis for the z-component of spin operator $S_z(t)$, Eq. (26). Shown are absolute values of the coefficient of expansion $|d_1|$ (blue line, left axis) and difference between eigenmodes $|\omega_1 - \omega_2|$ (red line, right axis) for results of simulations performed within (a) standard Bloch QME, (b) generalized Bloch QME with dissipation included, and (c) non-Markov generalized Bloch QME with dissipation included.

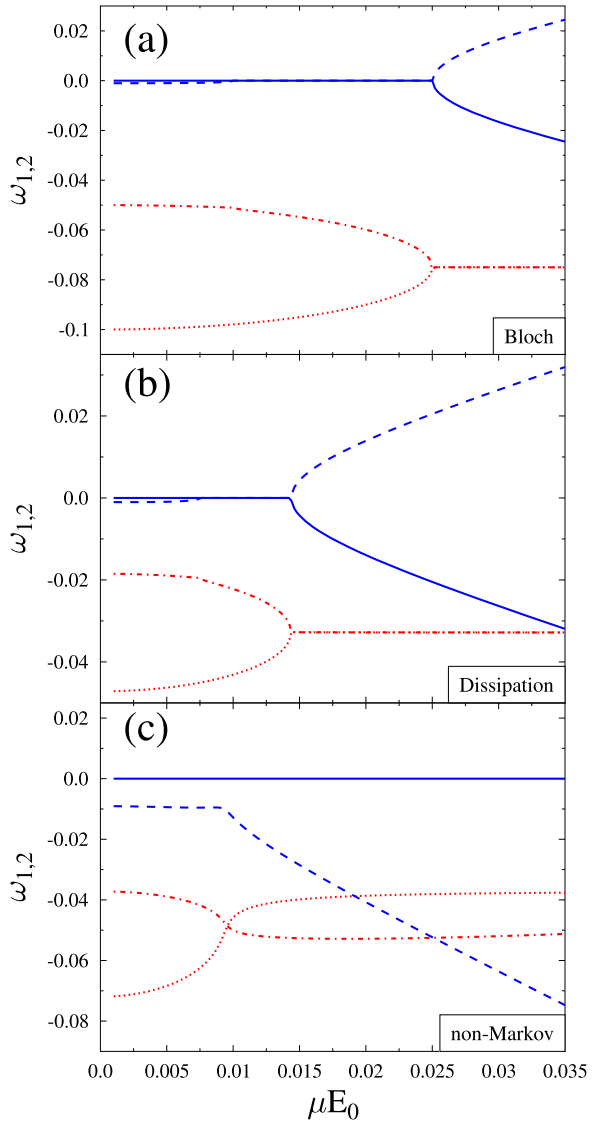


**FIG. 4.** Eigenmodes $\omega_1$ and $\omega_2$ vs coupling to the driving field $\mu E_0$. Shown are real (blue solid and blue dashed lines) and imaginary (red dashed and red dashed–dotted lines) parts of the eigenmodes for $S_z(t)$ simulations performed within (a) standard Bloch QME, (b) generalized Bloch QME with dissipation included, and (c) non-Markov generalized Bloch QME with dissipation included.

Figure 4 shows two eigenmodes that become degenerate at exceptional points. One sees that for the standard (panel a) and the generalized (panel b), Markov QME weak coupling to the driving field (below the LEP) corresponds to situations where real parts of the eigenmodes coincide while imaginary parts are different. Stronger couplings (above the LEP) correspond to zero differences in imaginary parts and different real parts. Note that similar behavior at LEP yields a transition between diffusive and ballistic motion[34,35] and an enhancement of the decoherence rate.[36–38] The behavior of eigenmodes for results obtained within non-Markov QME (panel c) is more complicated. No degeneracy is observed between the modes. Similarly, eigenmode analysis for the NEGF results yields a large number of modes (~50) with no LEPs present.

The absence of exceptional points in the results of non-Markov evolution is expected because the EOM for $S_z(t)$ is not generated by the time-independent Liouvillian anymore. One can understand the absence of the LEPs in this case from a purely mathematical perspective. Indeed, even if one starts from a time-dependent characteristic for a LEP [for example, for LEP2, one expects to have $\rho(t) \sim (d_1 + d_2 t)e^{-i\lambda t}$], the first step of time evolution will annihilate the LEP time dependence due to the convolution of the density operator with the time-dependent function, Eq. (25). Indeed, taking the integral in Eq. (25) with the memory kernel, which depends on time in a complicated way, does not preserve the original form of

$\rho(t)$. This can be easily seen by expanding the kernel in a Fourier series and performing time integration.

Failure of the concept of the Liouvillian exceptional point for non-Markov evolution is even more obvious when analyzing the more rigorous NEGF formulation, Eqs. (6)–(8). Indeed, on the right side of the Dyson equation, one has the product of two Green's functions: one from Eq. (6) and the other from Eq. (7). In principle, one could start from Eqs. (6)–(8) and apply the generalized Kadanoff–Baym ansatz to these expressions. This would yield an analog of QME that differs from (but is more accurate than) the Bloch QME. Such an equation would contain $\rho^2$ on its right side, which obviously indicates that the form $\rho(t) = (d_1 + d_2 t)e^{-i\lambda t}$ does not survive in a non-Markov formulation.

We note that the central parameters for the accuracy of the Markov approximation are the characteristic times of bath $t_c^B$ and system $t_c^S$ dynamics: the Markov approximation is accurate when $t_c^B \ll t_c^S$. For the model, $t_c^B$ is defined by the bandwidth $W_B$, temperature $T$, and structure of the bath spectral function $J(\omega)$: $t_c^B \sim \hbar/W$, $\hbar/k_B T$. The characteristic time of system dynamics is defined by the intra-system energy parameters (inter-level separation $\omega_{21}$, driving frequency $\omega_0$, detuning $\Delta$) and by the dissipation rate due to coupling to the bath (e.g., $\Gamma_{12,12}$): $t_c^S \sim 2\pi/\omega_{21}, 2\pi/\omega_0, 2\pi/\Delta, \hbar/\Gamma_{12,12}$.

## IV. CONCLUSION

We discuss the concept of Liouvillian exceptional points (LEPs) used in the description of the dynamics of open quantum systems. The discussion is focused on a model of a driven two-level system coupled to a thermal bath. Starting with an exact NEGF formulation of the problem and implementing a set of approximations, we derive the standard Bloch QME and its generalizations. The latter includes dissipation (retarded self-energy contribution). One of the generalizations is non-Markov.

We compare this approach with our recent publication,[42] where a similar analysis for the Hamiltonian exceptional points (HEPs) was carried out. We note that both HEP and LEP approximations rely on the Markov description of the system's evolution. In terms of neglected self-energies, standard HEP and LEP considerations are complementary: while HEP disregards lesser and greater projections of self-energy, standard LEP misses its retarded projection (dissipation).

By performing simulations for parameters previously shown to provide exceptional points,[43] we find that the generalized Bloch QME, which includes information about dissipation and treats evolution as a Markov process, is capable of providing LEPs, although for adjusted parameters. The non-Markov character of evolution does not permit the introduction of the concept of LEPs. In particular, neither the non-Markov Bloch QME formulation nor the NEGF formulation is capable of producing the LEPs. This inability to use LEPs for the description of non-Markov evolution is quite general. The concept of Liouvillian exceptional points can be introduced only for Markovian dynamics.

We note that while the RWA should be used in the derivation of the Bloch QME, within the NEGF treatment, the approximation may be relaxed. Such a more general consideration will not affect the conclusions. Indeed, the inability to introduce LEPs directly follows from the fact that the time-dependent characteristic expected for a LEP does not survive the non-Markov time evolution of the system. The absence of the RWA will only change a form of time-dependent function convolution, which will destroy the expected LEP time dependence. Similarly, as long as system evolution is non-Markov, the conclusions hold for any driving frequency or in the absence of external driving.

Finally, we stress that our work does not challenge existing experimental observations, some of which are mentioned in the introduction. We discuss the theoretical treatments used for the explanation of those experiments and indicate possible pitfalls of the theory. For example, in many cases, theoretical treatments utilizing Markov description and employing exceptional point analysis will predict an abrupt 'phase transition' when crossing the exceptional point. In reality (i.e., within a more accurate theoretical analysis), the transition between two different regimes will be smooth. The importance of the difference between the two (approximate and more accurate) theoretical descriptions and whether the approximate (Markov) treatment may lead to qualitative failures depends on the observables of interest.

## ACKNOWLEDGMENTS

This material is based upon work supported by the National Science Foundation under Grant No. 2154323.

## AUTHOR DECLARATIONS

### Conflict of Interest

The authors have no conflicts to disclose.

### Author Contributions

**Nikhil Seshadri**: Formal analysis (equal); Investigation (equal); Validation (equal); Writing – review & editing (equal). **Anqi Li**: Writing – review & editing (supporting). **Michael Galperin**: Formal analysis (equal); Investigation (equal); Methodology (lead); Project administration (lead); Validation (lead); Writing – original draft (lead); Writing – review & editing (lead).

## DATA AVAILABILITY

The data that support the findings of this study are available within the article.

## APPENDIX A: DERIVATION OF EQ. (7)

We start from the definition of the single-particle Green's function, Eq. (4). Taking the derivative in the first contour variable yields

$$i\frac{\partial}{\partial\tau_1}G_{ij}(\tau_1,\tau_2) = \delta_{i,j}\,\delta(\tau_1,\tau_2) + \sum_{n=1,2} H^S_{in}(t_1)\,G_{nj}(\tau_1,\tau_2) - i\sum_{n,\alpha}\Big[V_{ni,\alpha}\,\langle T_c\,\hat{d}_n(\tau_1)\hat{b}_\alpha(\tau_1)\,\hat{d}_j^\dagger(\tau_2)\rangle + \langle T_c\,\hat{b}_\alpha^\dagger(\tau_1)\hat{d}_n(\tau_1)\,\hat{d}_j^\dagger(\tau_2)\rangle\,V_{\alpha,in}\Big]. \quad \text{(A1)}$$

The first-order expansion of the scattering operator in the rightmost term of the expression leads to

$$i\frac{\partial}{\partial\tau_1}G_{ij}(\tau_1,\tau_2) = \delta_{i,j}\,\delta(\tau_1,\tau_2) + \sum_{n=1,2} H^S_{in}(t_1)\,G_{nj}(\tau_1,\tau_2) - i\sum_{n,n_1,n_2}\int_c d\tau\Big[\Pi_{ni,n_1n_2}(\tau_1,\tau) \times \langle T_c\,\hat{d}_n(\tau_1)\,\hat{d}^\dagger_{n_1}(\tau)\hat{d}_{n_2}(\tau)\,\hat{d}^\dagger_j(\tau_2)\rangle_0 + \Pi_{n_1n_2,in} \times (\tau,\tau_1)\,\langle T_c\,\hat{d}_n(\tau_1)\,\hat{d}^\dagger_{n_2}(\tau)\hat{d}_{n_1}(\tau)\,\hat{d}^\dagger_j(\tau_2)\rangle_0\Big]. \tag{A2}$$

Here, Π is defined in (8), and subscript 0 indicates evolution driven by the system Hamiltonian. Employing Wick's theorem to decouple multi-time correlation functions in the last term on the right side and dressing the result yields the Hartree–Fock approximation, Eq. (7).

## APPENDIX B: DERIVATION OF EQ. (10)

Here, we derive the exact EOM for the density matrix, Eq. (10), starting from the EOM for the Green's function (4).

We start by writing the left and right EOMs for the lesser projection of Green's function (4),

$$i\frac{\partial}{\partial t_1}G^<_{ij}(t_1,t_2) = \varepsilon_i G^<_{ij}(t_1,t_2) - \mu E(t_1)G^<_{ij}(t_1,t_2) + i\sum_{n,\alpha}\Big[V_{ni,\alpha}\langle\hat{d}^\dagger_j(t_2)\hat{d}_n(t_1)\hat{b}_\alpha(t_1)\rangle + V_{\alpha,in}\langle\hat{d}^\dagger_j(t_2)\hat{d}_n(t_1)\hat{b}^\dagger_\alpha(t_1)\rangle\Big], \tag{B1}$$

$$-i\frac{\partial}{\partial t_2}G^<_{ij}(t_1,t_2) = \varepsilon_j G^<_{ij}(t_1,t_2) - \mu E(t_2)G^<_{ij}(t_1,t_2) + i\sum_{n,\alpha}\Big[V_{jn,\alpha}\langle\hat{b}_\alpha(t_2)\hat{d}^\dagger_n(t_2)\hat{d}_i(t_1)\rangle + V_{\alpha,nj}\langle\hat{b}^\dagger_\alpha(t_2)\hat{d}^\dagger_n(t_2)\hat{d}_i(t_1)\rangle\Big]. \tag{B2}$$

Taking $t_1 = t_2 \equiv t$ and subtracting (B1) from (B2) yields

$$-i\frac{d}{dt}G^<_{ij}(t,t) = \omega_{ji}G^<_{ij}(t,t) - \mu E(t)\big[G^<_{ij}(t,t) - G^<_{ij}(t,t)\big] + \sum_{n,\alpha}\big[V_{ni,\alpha}\,G^<_{\alpha,nj}(t,t) + G^>_{jn,\alpha}(t,t)\,V_{\alpha,in} - V_{jn,\alpha}\,G^>_{\alpha,in}(t,t) - G^<_{ni,\alpha}(t,t)\,V_{\alpha,nj}\big]. \tag{B3}$$

Here,

$$G_{\alpha,m_1m_2}(\tau_1,\tau_2) \equiv -i\Big\langle T_c\,\hat{b}_\alpha(\tau_1)\big[\hat{d}^\dagger_{m_1}\hat{d}_{m_2}\big]^\dagger(\tau_2)\Big\rangle, \quad G_{m_1m_2,\alpha}(\tau_1,\tau_2) \equiv -i\Big\langle T_c\Big[\hat{d}^\dagger_{m_1}\hat{d}_{m_2}\Big](\tau_1)\;\hat{b}^\dagger_\alpha(\tau_2)\Big\rangle, \tag{B4}$$

are the mixed system-bath Green's functions that satisfy the Dyson equations

$$G_{\alpha,m_1m_2}(\tau_1,\tau_2) = \sum_{n_1,n_2}\int_c d\tau'\,F^{(0)}_\alpha(\tau_1,\tau') \times V_{\alpha,n_1n_2}\,G^{(2)}_{n_1n_2,m_1m_2}(\tau',\tau_2), \quad G_{m_1m_2,\alpha}(\tau_1,\tau_2) = \sum_{n_1,n_2}\int_c d\tau'\,G^{(2)}_{m_1m_2,n_1n_2}(\tau_1,\tau') \times V_{n_1n_2,\alpha}\,F^{(0)}_\alpha(\tau',\tau_2). \tag{B5}$$

Green's functions $F^{(0)}_\alpha$ and $G^{(2)}$ are defined in Eqs. (9) and (11), respectively.

Taking lesser and greater projections of (B5), setting $t_1 = t_2 \equiv t$, and substituting the resulting expressions into (B3) leads to (10).

## APPENDIX C: DERIVATION OF EQ. (13)

Here, we derive the Bloch equations, Eq. (13), starting from the exact EOM for the density matrix, Eq. (10).

Substituting the Kadanoff–Baym ansatz Eq. (12) into (10) gives

$$\frac{d}{dt}\rho_{ij}(t) \approx i\omega_{ji}\rho_{ij}(t) - i\mu E(t)\big[\rho_{ij}(t) - \rho_{ij}(t)\big] - i\sum_{n,n_1,n_2}\int_{-\infty}^{t}dt'\Big[\Pi^>_{ni,n_1n_2}(t-t')\,e^{i\omega_{jn}(t-t')}\Big\langle\Big[\hat{d}^\dagger_j\hat{d}_n\hat{d}^\dagger_{n_1}\hat{d}_{n_2}\Big](t')\Big\rangle - \Pi^<_{ni,n_1n_2}(t-t')\,e^{i\omega_{jn}(t-t')}\Big\langle\Big[\hat{d}^\dagger_{n_1}\hat{d}_{n_2}\hat{d}^\dagger_j\hat{d}_n\Big](t')\Big\rangle - \Pi^>_{jn,n_1n_2}(t-t')\,e^{i\omega_{ni}(t-t')}\Big\langle\Big[\hat{d}^\dagger_n\hat{d}_i\hat{d}^\dagger_{n_1}\hat{d}_{n_2}\Big](t')\Big\rangle + \Pi^<_{jn,n_1n_2}(t-t')\,e^{i\omega_{ni}(t-t')}\Big\langle\Big[\hat{d}^\dagger_{n_1}\hat{d}_{n_2}\hat{d}^\dagger_n\hat{d}_i\Big](t')\Big\rangle + \Pi^>_{n_1n_2,nj}(t'-t)\,e^{i\omega_{in}(t'-t)}\Big\langle\Big[\hat{d}^\dagger_{n_2}\hat{d}_{n_1}\hat{d}^\dagger_n\hat{d}_i\Big](t')\Big\rangle - \Pi^<_{n_1n_2,nj}(t'-t)\,e^{i\omega_{in}(t'-t)}\Big\langle\Big[\hat{d}^\dagger_n\hat{d}_i\hat{d}^\dagger_{n_2}\hat{d}_{n_1}\Big](t')\Big\rangle - \Pi^>_{n_1n_2,in}(t'-t)\,e^{i\omega_{nj}(t'-t)}\Big\langle\Big[\hat{d}^\dagger_{n_2}\hat{d}_{n_1}\hat{d}^\dagger_j\hat{d}_n\Big](t')\Big\rangle + \Pi^<_{n_1n_2,in}(t'-t)\,e^{i\omega_{nj}(t'-t)}\Big\langle\Big[\hat{d}^\dagger_j\hat{d}_n\hat{d}^\dagger_{n_2}\hat{d}_{n_1}\Big](t')\Big\rangle\Big], \tag{C1}$$

where self-energy Π is defined in Eq. (8).

In the single electron subspace of the problem

$$\begin{aligned}
\langle \hat{d}_1^\dagger \hat{d}_1 \hat{d}_1^\dagger \hat{d}_1 \rangle &= \langle \hat{d}_1^\dagger \hat{d}_2 \hat{d}_2^\dagger \hat{d}_1 \rangle = \langle \hat{d}_1^\dagger \hat{d}_1 \rangle \equiv \rho_{11}, \\
\langle \hat{d}_2^\dagger \hat{d}_1 \hat{d}_1^\dagger \hat{d}_1 \rangle &= \langle \hat{d}_2^\dagger \hat{d}_2 \hat{d}_2^\dagger \hat{d}_1 \rangle = \langle \hat{d}_2^\dagger \hat{d}_1 \rangle \equiv \rho_{12}, \\
\langle \hat{d}_1^\dagger \hat{d}_1 \hat{d}_1^\dagger \hat{d}_2 \rangle &= \langle \hat{d}_1^\dagger \hat{d}_2 \hat{d}_2^\dagger \hat{d}_2 \rangle = \langle \hat{d}_1^\dagger \hat{d}_2 \rangle \equiv \rho_{21}, \\
\langle \hat{d}_2^\dagger \hat{d}_2 \hat{d}_2^\dagger \hat{d}_2 \rangle &= \langle \hat{d}_2^\dagger \hat{d}_1 \hat{d}_1^\dagger \hat{d}_2 \rangle = \langle \hat{d}_2^\dagger \hat{d}_2 \rangle \equiv \rho_{22},
\end{aligned} \tag{C2}$$

with all other averages zero.

Substituting (C2) in (C1) and employing a fast bath approximation

$$\begin{aligned}
\rho_{11}(t') &\approx \rho_{11}(t), \quad \rho_{12}(t') \approx \rho_{12}(t)\, e^{+i\omega_{21}(t'-t)}, \\
\rho_{22}(t') &\approx \rho_{22}(t), \quad \rho_{21}(t') \approx \rho_{21}(t)\, e^{-i\omega_{21}(t'-t)},
\end{aligned} \tag{C3}$$

and neglecting bath-induced couplings between populations and coherences leads to (13).

## APPENDIX D: DERIVATION OF EQ. (21)

Within the single-electron subspace of the problem, there is a simple one-to-one correspondence between the single-particle and many-body states of the system. This correspondence allows one to express the lesser and greater projections of the two-particle GF (11) as

$$\begin{aligned}
G^{(2)<}_{n_1n_2,n_3n_4}(t_1,t_2) &\equiv -i\langle \left[\hat{d}^\dagger_{n_3}\hat{d}_{n_4}\right]^\dagger(t_2)\left[\hat{d}^\dagger_{n_1}\hat{d}_{n_2}\right](t_1)\rangle \\
&= -i\theta(t_1-t_2)\langle\langle n_2n_1|\,\mathcal{U}(t_1,t_2)\,|\,\rho_{SB}(t_2)\,n_4n_3\rangle\rangle \\
&\quad - i\theta(t_2-t_1)\langle\langle n_3n_4|\,\mathcal{U}(t_2,t_1)\,|\,n_1n_2\,\rho_{SB}(t_1)\rangle\rangle, \\
G^{(2)>}_{n_1n_2,n_3n_4}(t_1,t_2) &\equiv -i\langle \left[\hat{d}^\dagger_{n_1}\hat{d}_{n_2}\right](t_1)\left[\hat{d}^\dagger_{n_3}\hat{d}_{n_4}\right]^\dagger(t_2)\rangle \\
&= -i\theta(t_1-t_2)\langle\langle n_2n_1|\,\mathcal{U}(t_1,t_2)\,|\,n_4n_3\,\rho_{SB}(t_2)\rangle\rangle \\
&\quad - i\theta(t_2-t_1)\langle\langle n_3n_4|\,\mathcal{U}(t_2,t_1)\,|\,\rho_{SB}(t_1)\,n_1n_2\rangle\rangle,
\end{aligned} \tag{D1}$$

where the rightmost sides of the expressions are written in the Liouville space notation $|n_1n_2\rangle\rangle \equiv |n_1\rangle\langle n_2|$, $\hat{\rho}_{SB}$ is the total (system and bath) density operator and,

$$\mathcal{U}(t_1,t_2) \equiv T\,\exp\left[-i\int_{t_2}^{t_1} dt\;\mathcal{L}(t)\right], \tag{D2}$$

is the Liouville space evolution operator.

By decoupling the system and the bath dynamics with projection super-operator

$$\mathcal{P} \equiv \sum_{e,f} |ef\;\rho_B^{eq}\rangle\rangle\,\langle\langle ef\;I_B|, \tag{D3}$$

and introducing retarded and advanced Green's functions in Liouville space

$$\begin{aligned}
\mathcal{G}^r_{n_1n_2,n_3n_4}(t_1,t_2) &\equiv -i\theta(t_1-t_2)\langle\langle n_2n_1\,I_B|\,\mathcal{U}(t_1,t_2)\,|n_4n_3\,\rho_B^{eq}\rangle\rangle, \\
\mathcal{G}^a_{n_1n_2,n_3n_4}(t_1,t_2) &\equiv +i\theta(t_2-t_1)\langle\langle n_3n_4\,I_B|\,\mathcal{U}(t_1,t_2)\,|n_1n_2\,\rho_B^{eq}\rangle\rangle,
\end{aligned} \tag{D4}$$

one can rewrite the exact expressions (D1) in the form of a generalized Kadanoff–Baym ansatz in the Liouville space, Eq. (21).

Note that the expressions for the Green's functions in the Liouville space given by Eq. (22) are equivalent to their definition (D4) via

$$\mathcal{U}_{eff}(t_1,t_2) \equiv \langle\langle I_B|\,\mathcal{U}(t_1,t_2)\,|\rho_B^{eq}\rangle\rangle. \tag{D5}$$

## REFERENCES


[1] N. Moiseyev, *Non-Hermitian Quantum Mechanics* (Cambridge University Press, Cambridge, 2011).
[2] M.-A. Miri and A. Alù, Science **363**, eaar7709 (2019).
[3] S.-B. Lee, J. Yang, S. Moon, S.-Y. Lee, J.-B. Shim, S. W. Kim, J.-H. Lee, and K. An, Phys. Rev. Lett. **103**, 134101 (2009).
[4] C. E. Rüter, K. G. Makris, R. El-Ganainy, D. N. Christodoulides, M. Segev, and D. Kip, Nat. Phys. **6**, 192 (2010).
[5] C. Hahn, Y. Choi, J. W. Yoon, S. H. Song, C. H. Oh, and P. Berini, Nat. Commun. **7**, 12201 (2016).
[6] J. Doppler, A. A. Mailybaev, J. Böhm, U. Kuhl, A. Girschik, F. Libisch, T. J. Milburn, P. Rabl, N. Moiseyev, and S. Rotter, Nature **537**, 76 (2016).
[7] M. S. Ergoktas, S. Soleymani, N. Kakenov, K. Wang, T. B. Smith, G. Bakan, S. Balci, A. Principi, K. S. Novoselov, S. K. Ozdemir, and C. Kocabas, Science **376**, 184 (2022).
[8] Y. Wu, W. Liu, J. Geng, X. Song, X. Ye, C.-K. Duan, X. Rong, and J. Du, Science **364**, 878 (2019).
[9] J. Wiersig, Photonics Res. **8**, 1457 (2020).
[10] M. Yang, H.-Q. Zhang, Y.-W. Liao, Z.-H. Liu, Z.-W. Zhou, X.-X. Zhou, J.-S. Xu, Y.-J. Han, C.-F. Li, and G.-C. Guo, Sci. Adv. **9**, eabp8943 (2023).
[11] C. Liang, Y. Tang, A.-N. Xu, and Y.-C. Liu, Phys. Rev. Lett. **130**, 263601 (2023).
[12] J. Zhang, B. Peng, Ş. K. Özdemir, K. Pichler, D. O. Krimer, G. Zhao, F. Nori, Y.-x. Liu, S. Rotter, and L. Yang, Nat. Photonics **12**, 479 (2018).
[13] M. Naghiloo, M. Abbasi, Y. N. Joglekar, and K. W. Murch, Nat. Phys. **15**, 1232 (2019).
[14] T. Gao, E. Estrecho, K. Y. Bliokh, T. C. H. Liew, M. D. Fraser, S. Brodbeck, M. Kamp, C. Schneider, S. Höfling, Y. Yamamoto, F. Nori, Y. S. Kivshar, A. G. Truscott, R. G. Dall, and E. A. Ostrovskaya, Nature **526**, 554 (2015).
[15] G. Xu, X. Zhou, Y. Li, Q. Cao, W. Chen, Y. Xiao, L. Yang, and C.-W. Qiu, Phys. Rev. Lett. **130**, 266303 (2023).
[16] U. Günther, I. Rotter, and B. F. Samsonov, J. Phys. A: Math. Theor. **40**, 8815 (2007).
[17] I. Rotter, J. Phys. A: Math. Theor. **42**, 153001 (2009).
[18] M. C. Toroker and U. Peskin, J. Phys. B: At., Mol. Opt. Phys. **42**, 044013 (2009).
[19] R. Uzdin, A. Mailybaev, and N. Moiseyev, J. Phys. A: Math. Theor. **44**, 435302 (2011).
[20] W. D. Heiss, J. Phys. A: Math. Theor. **45**, 444016 (2012).
[21] S. Garmon, I. Rotter, N. Hatano, and D. Segal, Int. J. Theor. Phys. **51**, 3536 (2012).
[22] A. Delga, J. Feist, J. Bravo-Abad, and F. J. Garcia-Vidal, J. Opt. **16**, 114018 (2014).
[23] I. Rotter and J. P. Bird, Rep. Prog. Phys. **78**, 114001 (2015).
[24] C. Yang, X. Wei, J. Sheng, and H. Wu, Nat. Commun. **11**, 4656 (2020).
[25] G. Engelhardt and J. Cao, Phys. Rev. B **105**, 064205 (2022).
[26] L. Ferrier, P. Bouteyre, A. Pick, S. Cueff, N. Dang, C. Diederichs, A. Belarouci, T. Benyattou, J. Zhao, R. Su, J. Xing, Q. Xiong, and H. Nguyen, Phys. Rev. Lett. **129**, 083602 (2022).
[27] G. Engelhardt and J. Cao, Phys. Rev. Lett. **130**, 213602 (2023).
[28] Z.-Z. Li, W. Chen, M. Abbasi, K. W. Murch, and K. B. Whaley, Phys. Rev. Lett. **131**, 100202 (2023).
[29] A. Pick, S. Silberstein, N. Moiseyev, and N. Bar-Gill, Phys. Rev. Res. **1**, 013015 (2019).

[30]F. Minganti, A. Miranowicz, R. W. Chhajlany, and F. Nori, Phys. Rev. A **100**, 062131 (2019).
[31]F. Minganti, A. Miranowicz, R. W. Chhajlany, I. I. Arkhipov, and F. Nori, Phys. Rev. A **101**, 062112 (2020).
[32]I. I. Arkhipov, A. Miranowicz, F. Minganti, and F. Nori, Phys. Rev. A **102**, 033715 (2020).
[33]G. Chimczak, A. Kowalewska-Kudlaszyk, E. Lange, K. Bartkiewicz, and J. Peřina, Jr., Sci. Rep. **13**, 5859 (2023).
[34]K. Hashimoto, K. Kanki, S. Garmon, S. Tanaka, and T. Petrosky, Prog. Theor. Exp. Phys. **2016**, 053A02.
[35]K. Hashimoto, K. Kanki, S. Tanaka, and T. Petrosky, in *Non-Hermitian Hamiltonians in Quantum Physics*, edited by F. Bagarello, R. Passante, and C. Trapani (Springer International Publishing, Cham, 2016), pp. 263–279.
[36]W. Chen, M. Abbasi, Y. N. Joglekar, and K. W. Murch, Phys. Rev. Lett. **127**, 140504 (2021).
[37]S. Khandelwal, N. Brunner, and G. Haack, PRX Quantum **2**, 040346 (2021).
[38]J. Larson and S. Qvarfort, Open Syst. Inf. Dyn. **30**, 2350008 (2023).
[39]W. Chen, M. Abbasi, B. Ha, S. Erdamar, Y. N. Joglekar, and K. W. Murch, Phys. Rev. Lett. **128**, 110402 (2022).
[40]P. Kumar, K. Snizhko, Y. Gefen, and B. Rosenow, Phys. Rev. A **105**, L010203 (2022).
[41]J.-T. Bu, J.-Q. Zhang, G.-Y. Ding, J.-C. Li, J.-W. Zhang, B. Wang, W.-Q. Ding, W.-F. Yuan, L. Chen, Ş. Özdemir, F. Zhou, H. Jing, and M. Feng, Phys. Rev. Lett. **130**, 110402 (2023).
[42]S. Mukamel, A. Li, and M. Galperin, J. Chem. Phys. **158**, 154106 (2023).
[43]M. Am-Shallem, R. Kosloff, and N. Moiseyev, New J. Phys. **17**, 113036 (2015).
[44]N. Hatano, Mol. Phys. **117**, 2121 (2019).
[45]J. Perina Jr, A. Miranowicz, G. Chimczak, and A. Kowalewska-Kudlaszyk, Quantum **6**, 883 (2022).
[46]B. A. Tay, Physica A **620**, 128736 (2023).
[47]H. Haug and A.-P. Jauho, *Quantum Kinetics in Transport and Optics of Semiconductors*, 2nd Substantially Revised ed. (Springer, Berlin, Heidelberg, 2008).
[48]P. Lipavský, V. Špička, and B. Velický, Phys. Rev. B **34**, 6933 (1986).
[49]M. Esposito and M. Galperin, Phys. Rev. B **79**, 205303 (2009).
[50]M. Esposito and M. Galperin, J. Phys. Chem. C **114**, 20362 (2010).
[51]J. Fuchs, J. Main, H. Cartarius, and G. Wunner, J. Phys. A: Math. Theor. **47**, 125304 (2014).
[52]M. Frigo and S. G. Johnson, Proc. IEEE **93**, 216 (2005).
[53]A. Stan, N. E. Dahlen, and R. van Leeuwen, J. Chem. Phys. **130**, 224101 (2009).
[54]V. A. Mandelshtam and H. S. Taylor, J. Chem. Phys. **107**, 6756 (1997).